Voltaglue electroceutical adhesive patches for localized voltage stimulation

*Manisha Singh[1,2], Richard D. Webster[3], Terry W. J. Steele[1,2]**

[1]NTU-Northwestern Institute for Nanomedicine (NNIN), Interdisciplinary Graduate School (IGS), Nanyang Technological University (NTU), 50 Nanyang Drive, Singapore 637553

[2]School of Materials Science and Engineering (MSE), Division of Materials Technology, Nanyang Technological University (NTU), Singapore 639798

[3]Division of Chemistry and Biological Chemistry, School of Physical and Mathematical Sciences, Nanyang Technological University, Singapore 637371

*Correspondence to Terry W. J. Steele (e-mail: wjsteele@ntu.edu.sg)

KEYWORDS: Voltaglue, electroceuticals, voltage-mediated adhesives, electrocuring, bipolar

ABSTRACT: Electroceuticals have been proposed as nerve- and tissue-stimulating therapeutics for diverse ailments such as fracture repair, Parkinson's disease, diabetes, hypertension, and wound healing. However, academic and clinical investigation of electroceutical hypotheses remains intangible due to lack of suitable interfaces required for the application of uniform electric fields to localized tissues. There is an unmet need to develop materials that match the mechanical properties of soft tissues, are electrically conductive, and can flex to accommodate body movements. Herein, the design of a flexible resistive substrate and voltage-activated adhesive-

based ‘electroceutical plaster’ is demonstrated which generates bound electric fields. The electric fields generated by the resistive substrate can interact with the active component in the voltage-activated adhesive. Structure activity relationships of applied voltage and current bias on electrorheology and tissue adhesion are investigated. Electrocuring migration is observed where curing commences nearest the cathode and progresses towards the anode. A potential electroceutical dressing with a tunable lap shear adhesion of 20-65 kPa is introduced for evaluation of electroceutical therapies.

INTRODUCTION

Emergent therapeutic devices and wound dressings exercise exogenous static or dynamic electric fields to avert bacterial infection, prevent biofilm formation, and improve healing by galvanotaxis[1-4]. Investigations have explored direct current (DC), alternating current (AC), high-voltage pulsed current (HVPC), and low-intensity direct current (LIDC) to assist in fracture repair, pain management, and wound healing[3, 5]. For example, Griffin et al. stimulated pressure ulcer wounds with direct current via intermittent dosing of 200V for 20 consecutive days. Wound area reduction was significantly higher in the electrical stimulation group vs. placebo group[6]. Jankovic et al. modulated leg ulcer wounds with intermittent alternating voltages of 300 V for three weeks and reported wound area reduction increased by 36% in the case of electrical stimulation vs. control[7]. In most electrical stimulation studies, therapy has been provided by static, large-sized extracorporeal devices that do not interface to the tissue under investigation[6-8]. Hence, there is an unmet academic and clinical need for the miniaturization of electrical devices into implantable stimulators (e.g. electroceutical tapes) that allow systematic investigation for localized electrical stimulation[9-10]. Modern implantable stimulators use metals such as platinum, which is significantly

stiffer than the soft tissue with which it interfaces[11]. The development of materials that match the mechanical properties of soft tissues, are electrically conductive, and can flex to accommodate body movements would enable implants that are more readily accepted by the body[12]. Although there are a number of conductive hydrogels[13-16], they cannot form stable interconnect patterns in aqueous environments and require exotic fixation methods, such as perfluoropolyether (PFPE) to isolate microelectrodes[17]. Lightweight electroceutical tapes would allow flexible molding to tissue interfaces while controlling geometric, adhesive, and electrical parameters. However, this requires an on-demand, electrically conductive bioadhesive for bonding to the tissue interface. Bonding medical devices to wound sites without substrate failure is an existing unmet clinical challenge[18].

In regard to electroceutical devices, insufficient adhesion leads to erroneous electrical signals and exudate leakage near peri-wound skin[19]. Strong adhesion (>1 MPa) exacerbates wound pain due to soft tissue substrate failure—the newly formed tissue matrix is traumatized upon dressing removal. This delays healing, inflicts pain, and may lead to additional complications[18]. Wound dressings supporting tunable adhesion and cohesive failure are expected to provide low-risk wound trauma during dressing changes[20].

A new tool that electroceutical devices may be able to exploit is a voltage mediated adhesive (i.e., Voltaglue), previously shown to bond to wet tissues at low direct voltages of 5-10 V[21]. The composite films incorporate interdigitated electrodes (IDEs) and a voltage-activated bioadhesive with the advantages of wet and tunable tissue adhesion that displays a cohesive failure mechanism. The interdigitated electrodes serve to activate Voltaglue and allow electroceutical investigation[21]. However, bulk printing of IDEs with a resolution of 200-300 μm is limited by 3D printing inks in terms of toxic solvents, interfacial wetting, and limitations of printing viscous inks (~30 Pa.s). Further, Voltaglue activation is dependent on the gap thickness of electrodes and decaying

electrical field—all of which can change the mechanical properties of the bioadhesive unpredictably. A continuous electrode may overcome these limitations.

Teledeltos paper is a conductive substrate serves as a uniform, isotropic resistor (4-6 kohm. sq^{-1}) for creating simple, bounded electric fields[22-23]. Herein, it is hypothesized that Teledeltos paper will activate the Voltaglue if a contiguous anode/cathode configuration creates a bounded electric field. Taking advantage of the slow migration, an electroceutical model system is designed that allows a wave of Voltaglue activation that migrates from the cathode to anode. The adhesion is strong enough to fix the electroceutical device but can be peeled off without tissue substrate/matrix failure. The simple electroceutical model system is easily constructed and requires only two components (i) Teledeltos paper as the resistive substrate and (ii) a thin film of voltage-activated bioadhesive. This work elucidates the structure-activity relationships of geometry, electric fields, and constant currents on migration kinetics, real-time viscoelastic properties, and lap shear adhesion on soft tissue mimics. A fundamental mechanistic understanding is proposed to explain the migration from the cathode to the anode.

EXPERIMENTAL SECTION

MATERIALS

Generation 5 Polyamidoamine dendrimer (PAMAM G5, Mw=28.8 kDa) is purchased from Dendritech, Inc, USA. 3-[4-(bromomethyl) phenyl]-3-(trifluoromethyl)- diazirine (bromo-diazirine) is obtained from TCI, Japan. Teledeltos paper (PK-9025B) is procured from PASCO scientific, Roseville, CA.

METHODS

Synthesis of Voltaglue (i.e., PAMAM -g-diazirine)

PAMAM-g-diazirine (20 %) is prepared as previously published[21, 24]. PAMAM-g-diazirine (20%) bioadhesive is diluted (50 % w/w) with phosphate buffered saline (1X PBS) and referred to as "Voltaglue" throughout the text.

Preparation of Teledeltos paper electrodes

Teledeltos paper strips (40 x 10 mm) is coated with a carbon layer to prevent and delay water absorption with a JEOL sputter coater (JFC- 1600 Auto fine coater, 20 mA for 2 min). Silver ink, purchased from PASCO Scientific, USA or copper adhesive tape (5 x 10 mm strips), purchased from RS Components Pte Ltd, Singapore, and is applied to ensure proper electrical contacts with alligator clips. A bounded electrical field of 30 x 10 mm^2 remains. A thin layer (~30 mg) of Voltaglue (1 sq. cm) is applied equidistant from both copper adhesive tapes, as represented in **Figure S1**.

Evaluation of electrocuring progression

Electrocuring of Voltaglue on Teledeltos paper electrodes is stimulated via voltage feedback direct current (1, 2, or 3 mA), supplied with a source meter (2450 Keithley's Source Meter Unit). The Voltaglue progression is tracked through digital photography at 30 FPS and analyzed with ImageJ[25].

Electrorheology of Voltaglue activation on Teledeltos paper

Dynamic mechanical parallel plate analysis and real-time viscoelastic parameters are recorded with a modular rheometer (Physica MCR 102, Anton Paar, United States, 1% strain and 1 Hz

oscillation). Teledeltos paper/uncured Voltaglue composite is immobilized with a custom 3D-printed jig and fixed to the bottom plate (Peltier Universal Optical Device (P-PTD120 SN80670834)). A high impedance 10 mm ceramic probe (disposable plate D-PP10/MX/S07) is maintained at a gap thickness of 0.2 mm.

Lap shear adhesion evaluation on wet collagen substrates

Teledeltos paper electrodes and collagen films (2 x 2 cm^2) are mounted on a glass microscope slide with double-sided tape. Voltaglue (~30 mg) is sandwiched between the Teledeltos paper electrode and collagen substrate (Nippi, Japan)[26-27] and energized with 1, 2, or 3 mA DC for 10 min. Lap shear adhesion failure values are recorded at maximum stress before failure with a 50 N force cell (Chatillon Force Measurement Products, USA), with a linear elongation of 3 mm min^{-1}.

Quantitation of diazirine, G5-PAMAM, and M_w by size exclusion chromatography (SEC)

Polymer molar mass and radius of gyration are evaluated on an Agilent 1100 series high-performance liquid chromatography, coupled with a refractive index (RI) detector (mass quantitation) and a multi-angle laser light scattering (MALLS) detector (Wyatt MiniDawn, Wyatt Technology, USA). The column (Agilent PL Aquagel-OH Mixed H) had a 1% w/v formic acid eluent with a flow rate of 1 mL min^{-1}. PAMAM mass (dn/dc = 0.185) and diazirine mass (UV extinction coefficient at 350 nm= 1009.5 mL cm^{-1} g^{-1})[28] are recorded and analyzed with Wyatt ASTRA software (Version 5.19.1), Wyatt Technology, Santa Barbara, CA, USA).

Statistical analysis

All data are presented as mean ± SD (n=3). The significance is assessed by one-way ANOVA with Tukey correction as a post-hoc test, carried out using OriginPro 2016 64-bit Software, where $p < 0.05$ (*) is defined significant.

RESULTS

Construction of Electroceutical Patch and Overview of Structure-Activity Relationships

Voltaglue is coated onto Teledeltos paper, where the linear placement of the electrical tape (solid-state electrodes) is assumed to create a linear, bounded electrical field. The electrical field generation can be explored in numerous approaches (DC, AC, HVPC, LIDC, etc.) but herein the scope is limited to simplified DC designs— either applied direct voltage (e.g. 60 V), with measurement of current or vice-versa (e.g. 1 mA as shown in **Figure S1**). Preliminary explorations indicated that the Teledeltos paper wicks moisture out of the Voltaglue, so this is prevented by sputter coating carbon. The carbon coating increases the water contact angle with no significant changes in sheet resistance, as seen in **Figure S2**. The resulting composite strips are referred to as "electroceutical patch" throughout the text. Electrocuring progression on electroceutical patches is assessed with digital photography (30 FPS), observing the progression of the gas emitting cured Voltaglue (opaque) versus the transparent uncured Voltaglue. Viscoelastic sample properties are quantified via real-time rheology, with the dynamic mechanical analysis aided by a non-conductive ceramic probe with GΩ resistance. The ceramic probe prevents perturbations of the electric field and also limits any potential electrochemical reactions that could occur with metal probes. The electroceutical patch is evaluated on wet collagen substrates that served to mimic the wet substrates found in wounds and organ surfaces. The lower limit of functional adhesion strength is defined at

10 kPa or 100 g per sq. cm. This is the minimal force estimated to immobilize electroceutical or electrode patches and is the bond strength of commercial fibrin sealants.

Electroceutical Patch Activation Progresses from Cathode to Anode

Teledeltos electrodes direct the current to a polarized electric field. Cathode and anode terminals are defined by the silver ink/copper adhesive placement, with the Teledeltos paper serving as the conductive matrix between the two electrodes. Silver ink is easy to apply, but repeated use of alligator clips delaminate it. Copper adhesive tapes are more robust for on-going investigations and ensure proper electrical contact. As the conductive interface is only a means to setup the polarized field and no contact is made with the the liquid adhesive, the composition of the metal films isnt expected to affect Voltaglue activation. To confirm that an electric field is generated, Voltaglue is applied over a Teledeltos strip (4 x 1 sq. cm) by two means i) three segregated (5 µL, diameter 2 mm) drops of Voltaglue and, (ii) the same amount in a continuous line (width x length= 1.7 mm x 6.5 mm) as set up in **Figure 1A**. This simple experiment assesses for a linear, bounded electric field, utilizing a simple and inexpensive DC power supply. If present, the three segmented drops should be activated independently of their position within the *constant* electric field (constant current requires a dynamic electric field and is discussed in the next section). After a voltage gradient of 3 V mm^{-1} (60 V over 20 mm length) is applied, the 3 segmented drops are activated simultaneously, with electrocuring first polarized at the cathode. The curing progresses from the cathode (-) to the anode (+) as shown in **Figure 1A** after 0.5 and 5 min. Complete electrocuring is observed after 0.5 min with the continuous drop, whereas the segmented drops need 5 min for complete progression. This is speculated to result from the total moles of ions available, the curing dependence on volume/area ratios, the potential difference across the length (2 mm for segmented, 6.5 mm for continuous), or combinations thereof. To fix the geometry and

avoid dependencies of unknown parameters, a planar two-dimensional model system is employed further. The electroceutical patch has a 1 cm^2 film of Voltaglue (30 mg, thickness 500 µm) placed equidistant of both electrodes, as shown in **Figure 1B**. At 2 V mm^{-1}, (60V over 30 mm length) Voltaglue progresses with a suitable linear wavefront from the cathode to the anode. Constant voltage results in only 38 % curing (assessed by surface area) after 10 min. Complete curing is hypothesized to require a constant current source, which is investigated in the next section.

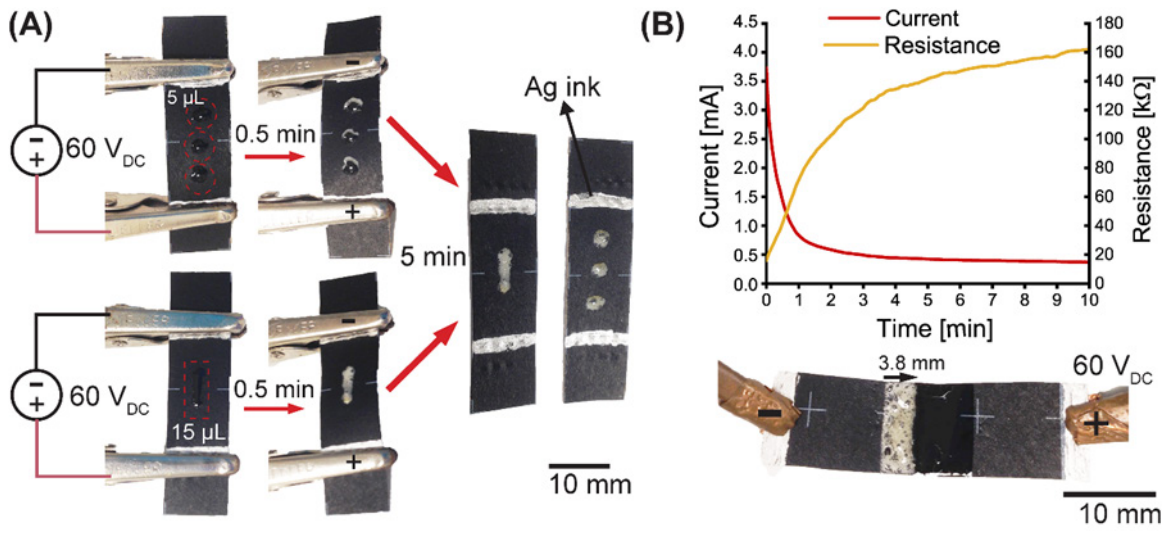

Figure 1. Electrocuring illustration on a continuous strip of Teledeltos paper. A) Voltaglue is activated on the surface of the semiconductive Teledeltos paper via two strategies- three segregated drops (diameter 2 mm) and continuous line (width x length = 1.7 mm x 6.5 mm). B) Progression of electrocuring on the surface of untreated Teledeltos paper. The resistance of the composite patch increases as the curing progresses.

Electrocuring progression kinetics correlates with the magnitude of the constant current

Under the influence of direct voltage, electrocuring progresses from the cathode to the anode and resistance of the electroceutical patch increases. A constant electric field cannot produce a steady

current if the resistance of a system varies. It is hypothesized that constant current may result in electrocuring higher than 38 % (previous section). Therefore, a constant current source (source meter) is adopted to supply steady currents of 1, 2, and 3 mA in order to investigate changes in temporal and spatial progression. The progression of cured Voltaglue from the cathode to anode is visually evidenced due to the change in transparent (uncured Voltaglue) to opaque (cured), as demonstrated in **Figure 2A** and **Video 1** (10X speed). In order to quantify the progression, real-time electrocuring of the electroceutical patch is video recorded at 30 FPS and later processed with the aid of imageJ software. The amount of progression against time is plotted in **Figure 2B**. The maximum electrocuring progression achieved in case of 1, 2, and 3 mA is 7 (±0.5), 8 (±0.3), and 9 (±0.1) mm respectively, and the corresponding charges supplied at maximum activation is 0.6, 0.8, and 1.6 C. The replicates of the electrocuring progression are fitted with a concatenate function to calculate the rate constant (**Figure 2C**). The differential curves (dotted) are utilized to calculate the rate constants (k) which are 0.002 (± 0.0003), 0.008 (± 0.002), and 0.019 (± 0.006) s^{-1} for 1, 2, and 3 mA respectively. Representative voltage vs. time recordings under the application of steady currents are presented in **Figure 2D, 2E, and 2F**. In order to ensure that activated diazirine results in one-sided progression as evidenced visually by foaming, PAMAM, G5 is used as a control. Electrochemically activated PAMAM, G5 leads to random foaming as seen in **Figure 2E**. The difference in the voltage between the control (PAMAM, G5) and Voltaglue is displayed in **Figure 2G**. Exposure of the cured electroceutical patches to an open flame indicates it is an endothermic material. The gas bubbles did not ignite (no H_2), while the remaining Voltaglue matrix also did not ignite (no O_2). This supports the presumption that the grafted diazirines within Voltaglue electrochemically activates a crosslinking group and N_2 gas is evolved as a by-product.

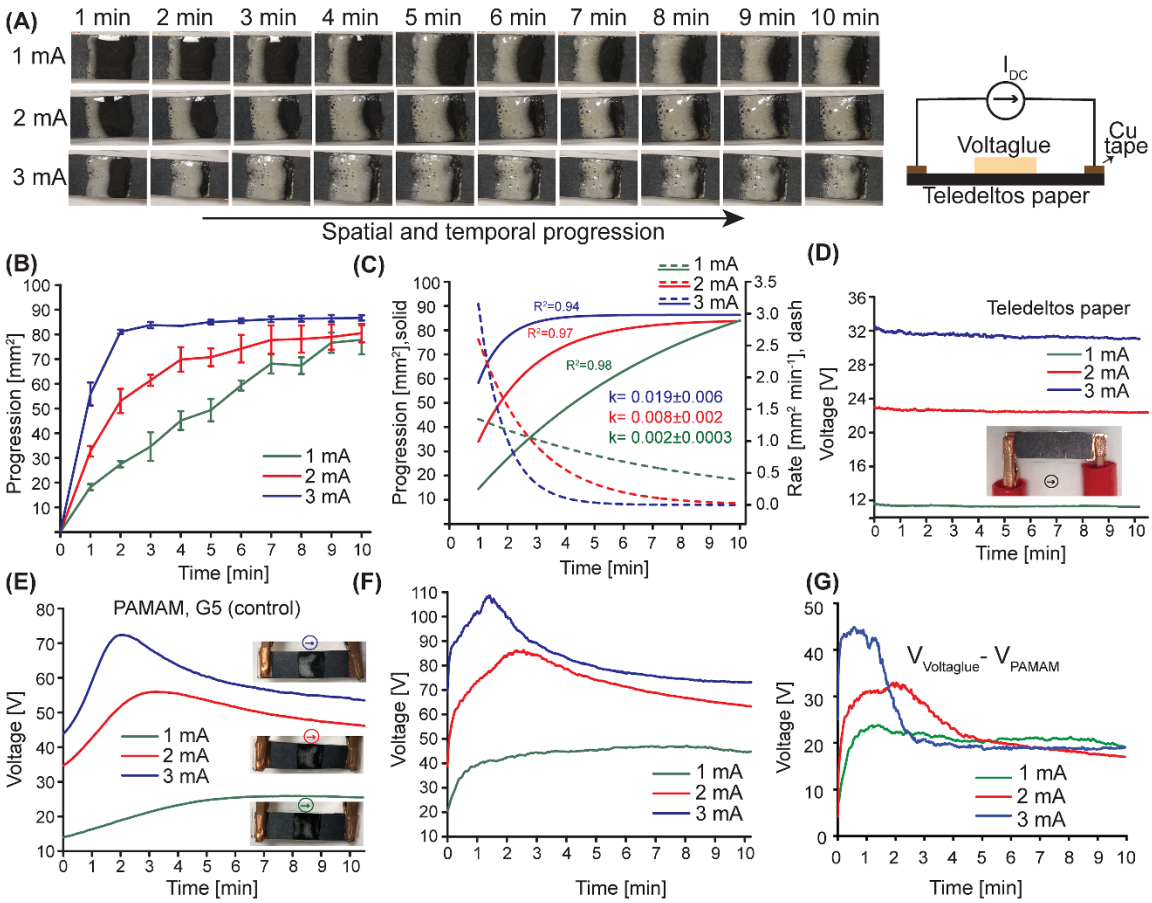

Figure 2. Electrocuring under constant current stimulation. A) Digital images of electrocuring progression over a 10-min interval under a constant current of 1 mA, 2 mA, or 3 mA. B) Surface area progression of electrocuring at constant current. C) Fitted curves and derived rate constants, k. D) Voltage recordings against the time of carbon-coated Teledeltos paper electrodes. E) Voltage recordings when a constant current is applied to PAMAM, G5 (control) liquid samples. F) Voltage recordings during electrocuring of Voltaglue. G) The difference in the voltage between the PAMAM, G5 (control) and Voltaglue as a function of constant current.

Constant current correlates with viscoelastic material properties

Real-time electrorheology is performed to assess the degree of crosslinking of Voltaglue on Teledeltos paper, under application of steady currents of 1, 2, or 3 mA. The corresponding changes

in the storage (G') and loss (G") moduli are recorded in real time with a custom electrorheometry setup as shown in **Figure 3A**. To avoid any interference of the electric field by the rheometer's internal ground, a ceramic probe (electrical resistance > GΩ) applied the sinusoidal shear strain to record the dynamic mechanical properties. PAMAM, G5 has no active crosslinker on its surface and serves as a non-modified control (no-grafted diazirine). Voltaglue on Teledeltos paper electrodes are assessed for G' and G" before direct current (DC) application as displayed in the region I in **Figure 3B**. Within region I, hydrogen bonding or other attractive forces are disrupted by the 1% strain oscillations at 1 Hz frequency. After the application of direct current, the crossover of G′ and G″ is observed and a sudden increase in the G' values is recorded as displayed in region II in **Figure 3B,** whereas no significant rise in G' is noted in the case of the control (no-diazirine grafting, no crosslinking). The electrocuring kinetics of Voltaglue from **Figure 3C** are replotted as a vector plot to explore the viscoelastic properties before, during, and after curing. A diagonal line marks the gelation point, defined as G" divided by G' or tan delta = 1. This also serves to divide the regions into the liquid (above) and solid-like regions (below the line). Voltaglue progresses from the liquid-like region and transitions into the solid-like material properties with an elastic modulus near kPa values. Uncured G" values can vary depending on the shear history (thixotropic fluid), but the G' values are similar. Gelation time and current magnitude inversely correlated (Pearson's r: -0.99), as presented in **Figure 3D**. The fastest gelation time of 2 min is observed at 3 mA. Storage modulus (after 9 min) also correlated (Pearson's r: 0.94) with the current applied, as summarized in **Figure 3E**.

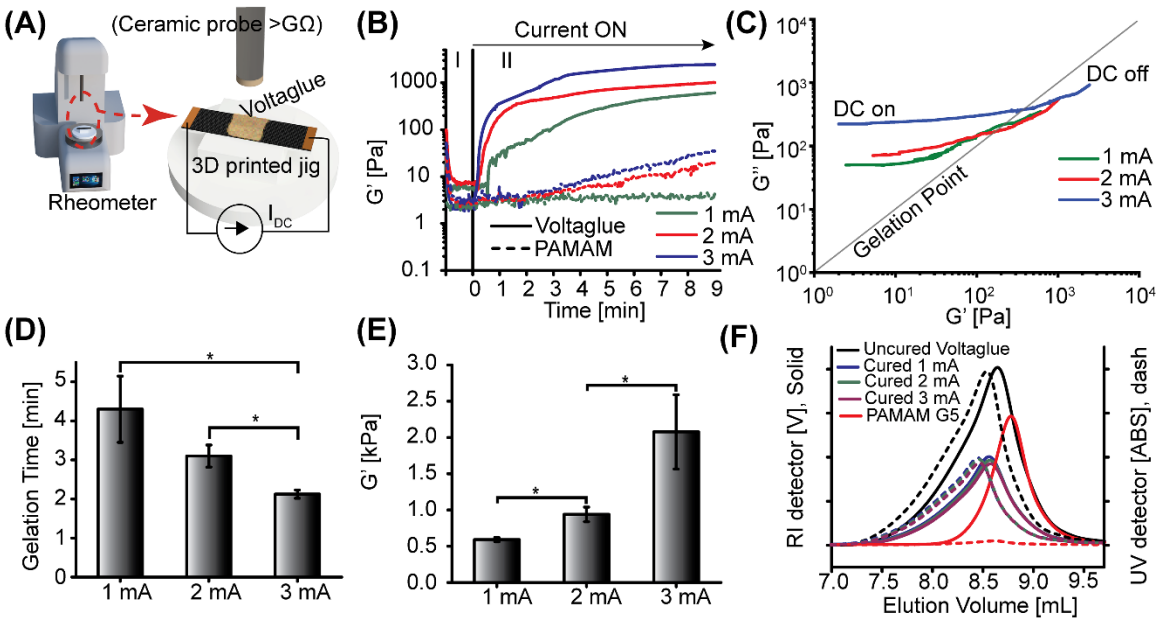

236

237 **Figure 3**. Real-time electrorheometry of electroceutical Patch. A) Electrorheology setup is
238 performed with the aid of a 3D-printed jig, to immobilize the carbon-coated Teledeltos composite.
239 Parallel plate and ceramic probe (10 mm d.) have a set sample gap of 0.3 mm. B) Storage modulus
240 (G') before and after constant current stimulation PAMAM, G5- and Voltaglue-Teledeltos paper
241 composites. C) G' vs. G" vector plots demonstrate the transition from liquid to viscoelastic states.
242 D) Gelation time (defined as the time to reach G"/G' = 1) ver-sus constant current applied. E)
243 Storage modulus after cessation of constant current off (9 min). F) SEC-MALS-UV signals
244 recorded for PAMAM, G5 (control), uncured Voltaglue, and electrocured Voltaglue: UV
245 absorbance measured at 350 nm, signals for electrocured Voltaglue are measured after 10 min of
246 electrocuring. Data presented as mean ± SD, n = 3, p-values are calculated using one-way ANOVA
247 with Tukey correction, *$p < 0.05$.

248

249

Soluble leachate determines half of the mass is not crosslinked, independent of the current magnitude

The experimental mass of recovered diazirine from the electroceutical patch is evaluated by size exclusion chromatography (SEC). Soluble leachate from the electrocured electroceutical patch is dissolved in 1% formic acid to evaluate unreacted Voltaglue. UV absorption peaks (dash lines) assessed the grafted-diazirine ($\varepsilon_{diazirine} >> \varepsilon_{PAMAM}$) and refractive index (RI) peaks assessed the PAMAM polymer (mass of diazirine < 5% PAMAM mass), as shown in **Figure 3F**. Grafted diazirine, PAMAM mass, and the conjugated molar mass for each formulation are listed in **Table 1.** The diazirine and PAMAM mass recovered after curing are reduced to ~50% for all current activations. The GPC analysis indicates that the leachate consists of uncured Voltaglue, which is likely from the matrix furthest away from the electric field/Teledeltos paper (at the air/Voltaglue interface).

Table 1. Summary of SEC-MALS-UV characterization of Electroceutical patch

Sample	AUC RI (RIU min) x 10-5	AUC UV (ABS min) x 10-2	Elution peak (mL)	Mw (kDa)[a]	Diazirine Mass (μg)[b]	PAMAM Mass (μg)[c]	Mass Ratio[d]	Mw/Mn
PAMAM G5	2.72	0.09	8.78	37 (±1)	0 ±0.21	148	-	1.01
Uncured Voltaglue	6.06	5.98	8.76	113 (±1)	9.70	327	33.71	1.95
Cured Voltaglue, 1mA	2.95	2.94	8.68	130 (±1)	5.30	160	30.19	2.02
Cured Voltaglue, 2mA	2.84	2.86	8.69	130 (±1)	5.13	154	30.01	1.96
Cured Voltaglue, 3mA	2.72	2.73	8.69	130(±1)	5.08	147	28.94	1.92

[a] Weight averaged molecular weight calculated through Multi-angle laser light scattering (MALLS) and refractive index (RI) signal
[b] The conjugated mass of diazirine is calculated using the UV extinction coefficient at 350 nm, derived from Absorbance (ABS) signals, 50 mL injection
[c] The mass of PAMAM is calculated according to dn/dc (0.185) and the refractive index (RI) signal, 50 mL injection (error < 5%)
[d] PAMAM Mass/ Diazirine Mass

Total charge governs tunable adhesion from 20 kPa to 65 kPa against a soft tissue mimic

The adhesion strength of the electrochemically activated electroceutical patch against a soft tissue mimic (collagen films) is analyzed via lap shear adhesion as illustrated in **Figure 4A**. The applied current correlated (Pearson's r: 0.99) with the maximum adhesion strength at failure, as shown in **Figure 4B**. Cured Voltaglue exhibits mean lap shear strengths of 44 ±1, 52±5, and 61±3 kPa for 1, 2, and 3 mA respectively. Inspection after failure indicated a layer of cured Voltaglue on both the collagen film and Teledeltos electrode surface, which is supportive of cohesive failure as opposed to interfacial or substrate failure. The control (no current) has unusually high lap shear—26 kPa vs. 2 kPa with plastic electrodes[21]. This is attributed to the viscous formulation and water absorption by the Teledeltos paper. This is also supported in **Figure 4C** where viscous strain is observed. Stress-strain curves in **Figure 4C** demonstrate a transition from viscous behavior (uncured) to more elastic material properties with less plastic yield as current progress from 1 to 3 mA.

To explore the dependence of charge in electrocuring, Voltaglue progression is plotted as a function of coulombs charge (**Figure 4D)**. The charge delivered to the electroceutical patch is calculated by replotting **Figure 2B** with the 1, 2, or 3 mA data overlaid. This data suggests that the total charge is the more closely related parameter with respect to electrocuring progression and

material properties. This hypothesis is tested by activating the electroceutical patches with a controlled amount of coulombic charge (3 mA constant current) and evaluating the lap shear adhesion. The total charge correlates with the lap adhesion strength and exhibits a tunable adhesion from 20 kPa to 65 kPa, as reported in **Figure 4E**. Representative load curves as a function of charge and displacement are displayed in **Figure 4F**. As charge increases, viscous yield diminishes but increases in lap shear failure and elongation before breaks are observed.

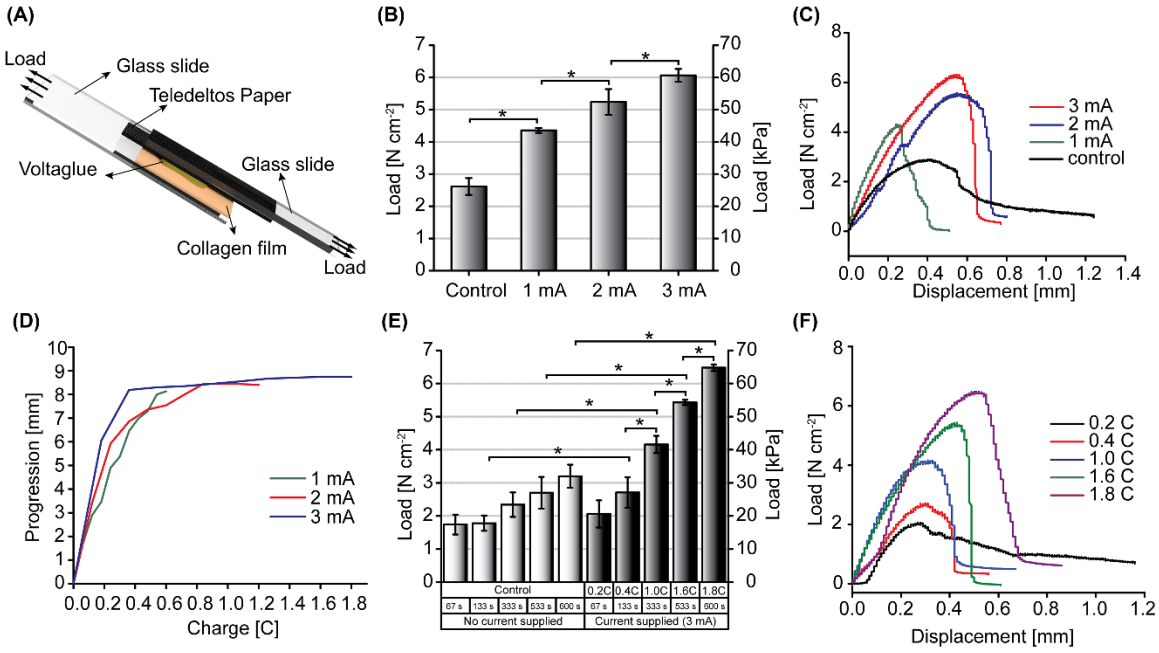

Figure 4. Lap shear adhesion dependence on current versus accumulative charge. A) Illustration of lap shear adhesion of electroceutical patch and wet collagen films, a soft tissue mimic (cit. 26). Red arrows indicate elongation vectors applied at an extension rate of 3 mm min^{-1}. B) Maximum adhesive shear strength at failure after 10 min of electrocuring. Control, no current applied. C) Load versus displacement curves. D) Figure 2B replotted as a function of charge. E) Maximum adhesive shear strength at failure at net charge delivered via a constant current of 3 mA. Time-based control, no charge provided. F) Corresponding load versus displacement curves. Data

presented as mean ± SD, n = 3, p-values are calculated using one-way ANOVA with Tukey correction, *p < 0.05.

DISCUSSION

The electroceutical patch is made possible with the following two components: 1) resistive Teledeltos paper and 2) Voltaglue as a bioadhesive. DC activated crosslinking of Voltaglue on the surface of Teledeltos paper migrates from the cathode to anode and was evaluated by measuring the increases in G' and G" where it changes from the viscoelastic liquid (10 Pa.s, 5 Pa) to solid (200 Pa.s, 2 kPa) states under an applied electric field. This has inferences on wound healing via electric fields where the electroceutical patch would allow the user to mold it to any wound's size and shape. Lap shear adhesion results indicate that the adhesion strength increases (20 to 65 kPa) across the DC values tested with an observed cohesive failure. Cohesive failure is meaningful in cases like chronic wounds where wound dressings are repeatedly applied to and removed from the same location of the skin, leading to skin stripping[19]. Thus, when the electroceutical patch is peeled off at stress failure, the adhesive matrix fails and a significant amount of Voltaglue would be left behind, preventing the shedding of newly formed tissues (accredited to the cohesive failure).

The electroceutical patch incorporates a bounded electric field (solid-state Teledeltos paper) that activates the Voltaglue droplets (liquid). The droplet edges become virtual polarized electrodes, analogous to bipolar electrochemistry where an electric field (supported in a liquid electrolyte) allows electrochemical reactions on polarized electrodes on solid conductors[29]. The length of the polarized electrodes modulates the kinetics, as shown in **Figure 1A**. The Teledeltos paper is an isotropic resister (**Figure 2D**) but loses its static conductivity when a concentrated solution of PAMAM or Voltaglue is applied (**Figure 2E and 2F**). This is due to moisture wicking in the

Teledeltos paper (despite carbon coating), PAMAM mediated charge repulsion, or combination thereof. Application of Voltaglue (PAMAM with grafted diazirine) requires an increase in voltage (electric field) in order to maintain the current (**Figure 2G**). As diazirine can reversibly be reduced (**Figure 5A**), the temporary rise in voltage in **Figure 2G** may be attributed to either of the following or combination thereof: 1) increased charge repulsion by the negatively charged diazirinyl radical, which is a known intermediate to form carbene[24, 30-32], 2) hydration of the Teledeltos paper, thus breaking the electrical percolation, 3) Nucleation and growth mechanisms in PAMAM[33], 4) resistance mismatch between the Teledeltos paper and Voltaglue (attributed to path of least resistance). The dissipation of voltage under all current conditions supports the hypothesis that the diazirinyl radical is consumed in a crosslinking reaction and nitrogen is evolved from cathode to anode. Conductivity differences between the paper and Voltaglue would generate a surface negative charge that would create an electrostatic gradient and cation (K^+ and Na^+) migration. The diffusion coefficients of the cations are speculated to be the major factor controlling progression kinetics (refer to **Table S1** in supporting information). As the complex modulus G* rises, cation diffusion becomes practically nonexistent. Thus, no further electrocuring can occur and all diffusing ions must migrate from uncured Voltaglue, as depicted in **Figure 5**. This accounts for the observation that a small residual strip of Voltaglue does not cure at the anode interface (**Figure 2A**), independent of the current.

This suggests a current-variable zone of activation at the cathode terminal and this zone migrates in response to cations migrating from uncured Voltaglue (**Figure 5B**). A steady-state is reached when the ions attain their equilibrium distribution near the virtual anode and cathode within the activation zone, dictated by the applied current. This process is simplified in **Figure 5B** where Teledeltos electrodes are divided into three zones: Blue zone—representing the cured Voltaglue,

Blue-Red gradient zone—representing the active electrocuring, Red zone--- representing the uncured Voltaglue and the source of migrating cations. Blue-Red gradient zone moves to the right as the electrocuring migrates towards the anode.

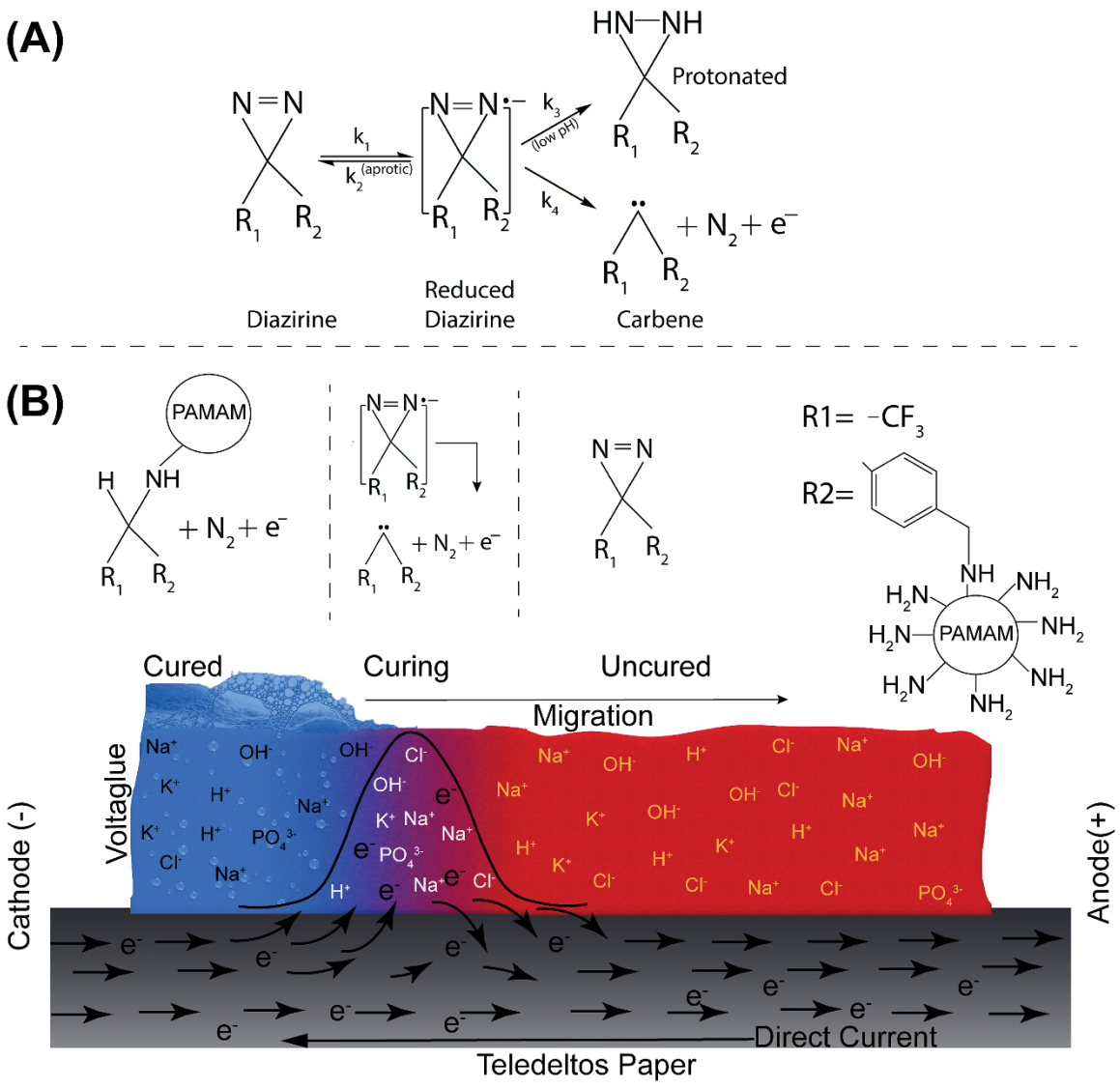

Figure 5. Rudimentary mechanism of electrocuring progression. A) Reaction illustrating the diazirine to diazirinyl radical to carbene cross-linking mechanism. B) Schematic showing the mechanism of electrocuring on electroceutical patch.

Electrocuring via Teledeltos paper permits engineering of a spot-based Voltaglue activation design, where each spot can be independently activated (**Figure 1A**). Independent spot-based designs, if electrically isolated from each other, can give additional freedom of applying a different type of stimulation (i.e. HPVC, DC, AC, LIDC or combination thereof) over different regions of wound surfaces at the same time.

Wound dressing in place during stimulation must be able to conduct sufficient electrical current to produce the desired effect on the wounded tissue. Bourguignon et al. have shown that most of the modern wound dressings have a resistivity higher than 10^9 ohm cm^2, thus making them unsuitable for direct application of electric stimulation using the currently available clinical electrical stimulators[34-35]. The electroceutical patch (resistivity: ~10^3 ohm cm^2) as tested could provide the tunable adhesion as per end-user demands, where Voltaglue activation by Teledeltos electrodes would be a considerable advantage. Thakral et al. have summarized the significance of electrical stimulation to accelerate wound healing[3]. For example, Peters et al. have shown 86 % reduction (vs. placebo) in wound area on diabetic ulcer wounds upon application of DC (50 V) via Dacron-mesh silver nylon stocking[36]. In another study, Houghton et al. have demonstrated 76 % reduction in wound area on pressure ulcer wounds in spinal cord injured patients upon application of HPVC (150 V, 10 Hz) using a silver nylon dressing (4.8 x 10.2 cm). Ud-Din et al. indicated that electrical stimulation accelerates acute cutaneous wound healing by inducing angiogenesis[37]. They applied 20-80 V, 60 Hz via an electrical stimulation device 'Fenzian system' (Fenzian Ltd, Hungerford, UK). All the above-mentioned designs apply electric field topically via skin only. Applied fields could change unpredictably due to change in the skin and tissue impedances before it reaches deep tissues[3-4, 34]. None of these device designs are suited for *in-vivo* implant translation where electric fields and currents can penetrate more deeply and locally into wounds. Nevertheless, the proposed

electroceutical patch needs further refinement before it can be translated for *in-vivo* applications since the immediate application is restricted by the unknown biocompatibility of Teledeltos paper. Effectiveness would increase if the Teledeltos paper could be replaced by other semiconductive biocompatible polymeric substrates, for example- PEDOT: PSS, polypyrrole, or graphene composites[38-44]. All of the above-mentioned wound healing cases require voltages in ranges of 30-300 V, but modern adhesives in wound healing are not tested under such voltage conditions. The electroceutical patch when utilized with 3 mA applied current, resulted in a voltage level of 110 V (**Figure 2F**) and did not cause any detrimental effects (e.g. burning or dissociation) to Voltaglue; rather it advanced the curing and adherence as tested under 10 min (**Figure 2-4**).

Many more potential applications exist outside of wound stimulation. DC pulses are exploited in electroporation to improve the insertion of drugs into tumors and DNA into cell nuclei[45-46]. In traditional electrically-assisted drug delivery systems (iontophoresis), electrodes are placed on the surface and a field is applied[47]. The simplicity of the Voltaglue electroceutical patch allows expansion into drug-depot applications, where the combination of gradient curing, dendrimer grafting and current transduction may be engineered for passive and on-demand drug delivery systems[48-51]. The strength of the electric field diminishes from the semiconductor surface. Hence, modulated electric fields would lead to electrocuring gradients that can be exploited in drug delivery applications in terms of partially and fully cured Voltaglue electraceuticals for variable rates of dendrimer/drug leaching.

A fundamental mechanism of the crosslinking is proposed, which relies on the assumption of carbene- based curing. One electron reduction of diazirine is well documented for reversible diazirinyl radical formation, which would be an intermediate for carbene[31-32, 52-55]. However, other cross-linking mechanisms cannot be excluded, including 1) Diazirinyl radicals dimerizing to form

aryl nitriles[31], 2) Diazirine/diazirinyl may isomerize into aryl diazo-intermediates that dimerize to form azines[56], 3) carbene attacks on diazirine to form azines and N_2 generation[57-58], 4) amine oxidation at the anode[59-60]. The proposed mechanism given in **Figure 5** is under continuous investigation as part of our future work. Further work will also address a more quantitative understanding of activation parameters such as the barriers for charge injection, the role of charge carrier mobilities under the influence of temperature, and AC electric fields in terms of curing migration from cathode to anode.

CONCLUSION

The electroceutical patch is designed to adhere directly to biological substrates, through a combination of Voltaglue (PAMAM-g-diazirine) activated with a semiconductor film. Teledeltos paper serves as a model flexible semiconductor, generating bounded electric fields for the voltage-activated adhesive. For the first time, virtual bipolar electrodes are formed in-situ, allowing independent activation of Voltaglue droplet within a polarized electric field. For the first time, electrocuring migration is observed that commences nearest the cathode (electron source) and progresses across the Voltaglue thin film towards the anode. Tunable lap shear adhesion from 20 - 65 kPa against a soft tissue mimic is obtained. The cohesive failure of the electroceutical patch prevents damage of soft substrates. The combination of Voltaglue and biocompatible semiconducting surfaces yields a new tool towards electraceutical medical devices and associated therapies.

ASSOCIATED CONTENT

Related **Video 1** is available free of charge on the ACS Publications Website. The **Supporting Information** is available free of charge on the ACS Publications website. A real-time video

illustrating the migration of Voltaglue activation from cathode to anode, experiment section, design and geometry information, instrumentation (contact angle and four-point probe test).

AUTHOR INFORMATION

Corresponding Author

*Correspondence to Terry W. J. Steele (e-mail: wjsteele@ntu.edu.sg)

Funding Sources

This work was financially supported by the Ministry of Education (Singapore) Tier 2 Grant: Reversible, electrocuring adhesives (MOE2014-T2-2-100), NTU-Northwestern Institute for Nanomedicine Grant: 3D-Printing of Electro-Curing Nanocomposite Living Electrodes for Cardiac Tissue Regeneration, Agency for Science, Technology and Research (A*Star) IRG17283008 'Microprocessor based methods of composite curing'

ACKNOWLEDGMENT

The authors acknowledge the financial support from the Ministry of Education (Singapore) Tier 2 Grant: Reversible, electrocuring adhesives (MOE2014-T2-2-100), NTU-Northwestern Institute for Nanomedicine Grant: 3D-Printing of Electro-Curing Nanocomposite Living Electrodes for Cardiac Tissue Regeneration, Singapore Agency for Science, Technology and Research (A*STAR) AME IRG grant (IRG17283008). The authors would like to thank NTU-Interdisciplinary Graduate School scholarship program, and School of Materials Science and Engineering for all the research facilities provided.

REFERENCES

1. Aljghami, M. E.; Saboor, S.; Amini-Nik, S., Emerging Innovative Wound Dressings. *Ann Biomed Eng* **2019,** *47* (3), 659-675.

2. Barki, K. G.; Das, A.; Dixith, S.; Ghatak, P. D.; Mathew-Steiner, S.; Schwab, E.; Khanna, S.; Wozniak, D. J.; Roy, S.; Sen, C. K., Electric Field Based Dressing Disrupts Mixed-Species Bacterial Biofilm Infection and Restores Functional Wound Healing. *Ann Surg* **2017,** 269(4), 756–766.

3. Thakral, G.; Lafontaine, J.; Najafi, B.; Talal, T. K.; Kim, P.; Lavery, L. A., Electrical stimulation to accelerate wound healing. *Diabet Foot Ankle* **2013,** *4*, 1-9.

4. Houghton, P. E., Electrical stimulation therapy to promote healing of chronic wounds: a review of reviews. *Chronic Wound Care Management and Research* **2017,** *Volume 4*, 25-44.

5. Banerjee, J.; Das Ghatak, P.; Roy, S.; Khanna, S.; Sequin, E. K.; Bellman, K.; Dickinson, B. C.; Suri, P.; Subramaniam, V. V.; Chang, C. J.; Sen, C. K., Improvement of human keratinocyte migration by a redox active bioelectric dressing. *PLoS One* **2014,** *9* (3), e89239.

6. Griffin, J. W.; Tooms, R. E.; Mendius, R. A.; Clifft, J. K.; Vander Zwaag, R.; el-Zeky, F., Efficacy of high voltage pulsed current for healing of pressure ulcers in patients with spinal cord injury. *Physical therapy* **1991,** *71* (6), 433-42; discussion 442-444.

7. Jankovic, A.; Binic, I., Frequency rhythmic electrical modulation system in the treatment of chronic painful leg ulcers. *Arch Dermatol Res* **2008,** *300* (7), 377-383.

8. Torkaman, G., Electrical Stimulation of Wound Healing: A Review of Animal Experimental Evidence. *Adv Wound Care (New Rochelle)* **2014,** *3* (2), 202-218.

9. Mishra, S., Electroceuticals in medicine - The brave new future. *Indian Heart J* **2017,** *69* (5), 685-686.

458 10. Saxena, T.; Bellamkonda, R. V., Implantable electronics: A sensor web for neurons. *Nat*
459 *Mater* **2015,** *14* (12), 1190-1191.
460 11. Prodanov, D.; Delbeke, J., Mechanical and Biological Interactions of Implants with the
461 Brain and Their Impact on Implant Design. *Frontiers in Neuroscience* **2016,** *10*, 1-20.
462 12. Viventi, J.; Kim, D.-H.; Moss, J. D.; Kim, Y.-S.; Blanco, J. A.; Annetta, N.; Hicks, A.;
463 Xiao, J.; Huang, Y.; Callans, D. J.; Rogers, J. A.; Litt, B., A Conformal, Bio-interfaced Class of
464 Silicon Electronics for Mapping Cardiac Electrophysiology. *Science translational medicine*
465 **2010,** *2* (24), 24ra22-24ra22.
466 13. Yuk, H.; Lu, B.; Zhao, X., Hydrogel bioelectronics. *Chem Soc Rev* **2019**,48, 1642-1667.
467 14. Han, L.; Yan, L.; Wang, M.; Wang, K.; Fang, L.; Zhou, J.; Fang, J.; Ren, F.; Lu, X.,
468 Transparent, Adhesive, and Conductive Hydrogel for Soft Bioelectronics Based on Light-
469 Transmitting Polydopamine-Doped Polypyrrole Nanofibrils. *Chemistry of Materials* **2018,** *30*
470 (16), 5561-5572.
471 15. Chai, Q.; Jiao, Y.; Yu, X., Hydrogels for Biomedical Applications: Their Characteristics
472 and the Mechanisms behind Them. *Gels* **2017,** *3* (1), 1-15.
473 16. Caló, E.; Khutoryanskiy, V. V., Biomedical applications of hydrogels: A review of
474 patents and commercial products. *European Polymer Journal* **2015,** *65*, 252-267.
475 17. Wang, Y.; Zhu, C.; Pfattner, R.; Yan, H.; Jin, L.; Chen, S.; Molina-Lopez, F.; Lissel, F.;
476 Liu, J.; Rabiah, N. I.; Chen, Z.; Chung, J. W.; Linder, C.; Toney, M. F.; Murmann, B.; Bao, Z., A
477 highly stretchable, transparent, and conductive polymer. Science Advances 2017, 3 (3),
478 e1602076.

18. Matsumura, H.; Imai, R.; Ahmatjan, N.; Ida, Y.; Gondo, M.; Shibata, D.; Wanatabe, K., Removal of adhesive wound dressing and its effects on the stratum corneum of the skin: comparison of eight different adhesive wound dressings. *Int Wound J* **2014,** *11* (1), 50-54.

19. Rippon, M.; White, R.; Davies, P., *Skin adhesives and their role in wound dressings*. 2007; Vol. 3, 76-86.

20. Klode, J.; Schottler, L.; Stoffels, I.; Korber, A.; Schadendorf, D.; Dissemond, J., Investigation of adhesion of modern wound dressings: a comparative analysis of 56 different wound dressings. *J Eur Acad Dermatol Venereol* **2011,** *25* (8), 933-939.

21. Singh, M.; Nanda, H. S.; O'Rorke, R. D.; Jakus, A. E.; Shah, A. H.; Shah, R. N.; Webster, R. D.; Steele, T. W. J., Voltaglue Bioadhesives Energized with Interdigitated 3D-Graphene Electrodes. *Adv Healthc Mater* **2018,** *7* (21), e1800538.

22. Physics, D. o. E. E. a. A. *Field Plotting Using Teledeltos Paper*; Aston University: 1994.

23. Pasco.com. https://www.pasco.com/prodCatalog/PK/PK-9025_conductive-paper-with-grid/index.cfm.

24. Ping, J.; Gao, F.; Chen, J. L.; Webster, R. D.; Steele, T. W., Adhesive curing through low-voltage activation. *Nat Commun* **2015,** *6*, 8050.

25. Schneider, C. A.; Rasband, W. S.; Eliceiri, K. W., NIH Image to ImageJ: 25 years of image analysis. *Nature Methods* **2012,** *9*, 671.

26. Nippi Collagen. http://nippicollagen.com/ (accessed 08 March 2019).

27. Steele, T. W. J.; Huang, C. L.; Nguyen, E.; Sarig, U.; Kumar, S.; Widjaja, E.; Loo, J. S. C.; Machluf, M.; Boey, F.; Vukadinovic, Z.; Hilfiker, A.; Venkatraman, S. S., Collagen-cellulose composite thin films that mimic soft-tissue and allow stem-cell orientation. *Journal of Materials Science-Materials in Medicine* **2013,** *24* (8), 2013-2027.

28. Feng, G.; Djordjevic, I.; Mogal, V.; O'Rorke, R.; Pokholenko, O.; Steele, T. W., Elastic Light Tunable Tissue Adhesive Dendrimers. *Macromol Biosci* **2016,** *16* (7), 1072-1082.

29. Fosdick, S. E.; Knust, K. N.; Scida, K.; Crooks, R. M., Bipolar electrochemistry. *Angew Chem Int Ed Engl* **2013,** *52* (40), 10438-10456.

30. Gan, L.; Tan, N. C. S.; Shah, A. H.; Webster, R. D.; Gan, S. L.; Steele, T. W. J., Voltage-Activated Adhesion through Donor–Acceptor Dendrimers. *Macromolecules* **2018,** *51* (17), 6661-6672.

31. Ge, S.-S.; Chen, B.; Wu, Y.-Y.; Long, Q.-S.; Zhao, Y.-L.; Wang, P.-Y.; Yang, S., Current advances of carbene-mediated photoaffinity labeling in medicinal chemistry. *RSC Advances* **2018,** *8* (51), 29428-29454.

32. Yamamoto, N.; Bernardi, F.; Bottoni, A.; Olivucci, M.; Robb, M. A.; Wilsey, S., Mechanism of Carbene Formation from the Excited States of Diazirine and Diazomethane: An MC-SCF Study. Journal of the American Chemical Society **1994**, 116 (5), 2064-2074.

33. Abdelhamid, M. E.; Snook, G. A., Conducting Polymers and Their Application in Supercapacitor Devices. In *Encyclopedia of Polymer Science and Technology*, 2018; pp 1-20.

34. Kloth, L. C., Electrical Stimulation Technologies for Wound Healing. *Adv Wound Care (New Rochelle)* **2014,** *3* (2), 81-90.

35. Bourguignon G.J., Marshall D.A., Chang K., Eaglstein W., Occlusive Wound Dressings Suitable for Use with Electrical Stimulation. *wounds* **1991,** *3* (3), 127-129.

36. Peters, E. J.; Lavery, L. A.; Armstrong, D. G.; Fleischli, J. G., Electric stimulation as an adjunct to heal diabetic foot ulcers: a randomized clinical trial. *Arch Phys Med Rehabil* **2001,** *82* (6), 721-725.

524 37. Ud-Din, S.; Sebastian, A.; Giddings, P.; Colthurst, J.; Whiteside, S.; Morris, J.;
525 Nuccitelli, R.; Pullar, C.; Baguneid, M.; Bayat, A., Angiogenesis is induced and wound size is
526 reduced by electrical stimulation in an acute wound healing model in human skin. *PLoS One*
527 **2015,** *10* (4), e0124502.
528 38. Liu, Y.; Zhang, B.; Xu, Q.; Hou, Y.; Seyedin, S.; Qin, S.; Wallace, G. G.; Beirne, S.;
529 Razal, J. M.; Chen, J., Development of Graphene Oxide/Polyaniline Inks for High Performance
530 Flexible Microsupercapacitors via Extrusion Printing. *Advanced Functional Materials* **2018,** *28*
531 (21), 1706592.
532 39. Pires, F.; Ferreira, Q.; Rodrigues, C. A.; Morgado, J.; Ferreira, F. C., Neural stem cell
533 differentiation by electrical stimulation using a cross-linked PEDOT substrate: Expanding the
534 use of biocompatible conjugated conductive polymers for neural tissue engineering. *Biochim*
535 *Biophys Acta* **2015,** *1850* (6), 1158-1168.
536 40. Yan, X.; Chen, J.; Yang, J.; Xue, Q.; Miele, P., Fabrication of free-standing,
537 electrochemically active, and biocompatible graphene oxide-polyaniline and graphene-
538 polyaniline hybrid papers. *ACS Appl Mater Interfaces* **2010,** *2* (9), 2521-2529.
539 41. Chen, H.; Müller, M. B.; Gilmore, K. J.; Wallace, G. G.; Li, D., Mechanically Strong,
540 Electrically Conductive, and Biocompatible Graphene Paper. *Advanced Materials* **2008,** *20* (18),
541 3557-3561.
542 42. George, P. M.; Lyckman, A. W.; LaVan, D. A.; Hegde, A.; Leung, Y.; Avasare, R.;
543 Testa, C.; Alexander, P. M.; Langer, R.; Sur, M., Fabrication and biocompatibility of polypyrrole
544 implants suitable for neural prosthetics. *Biomaterials* **2005,** *26* (17), 3511-3519.
545 43. Wang, D.-W.; Li, F.; Zhao, J.; Ren, W.; Chen, Z.-G.; Tan, J.; Wu, Z.-S.; Gentle, I.; Lu,
546 G. Q.; Cheng, H.-M., Fabrication of Graphene/Polyaniline Composite Paper via In Situ Anodic

547 Electropolymerization for High-Performance Flexible Electrode. ACS Nano 2009, 3 (7), 1745-
548 1752.
549 44. Jakus, A. E.; Secor, E. B.; Rutz, A. L.; Jordan, S. W.; Hersam, M. C.; Shah, R. N., Three-
550 Dimensional Printing of High-Content Graphene Scaffolds for Electronic and Biomedical
551 Applications. *ACS Nano* **2015,** *9* (4), 4636-4648.
552 45. Rosazza, C.; Meglic, S. H.; Zumbusch, A.; Rols, M. P.; Miklavcic, D., Gene
553 Electrotransfer: A Mechanistic Perspective. Current gene therapy 2016, 16 (2), 98-129.
554 46. Yarmush, M. L.; Golberg, A.; Sersa, G.; Kotnik, T.; Miklavcic, D., Electroporation-based
555 technologies for medicine: principles, applications, and challenges. *Annu Rev Biomed Eng* **2014,**
556 *16*, 295-320.
557 47. Roustit, M.; Blaise, S.; Cracowski, J. L., Trials and tribulations of skin iontophoresis in
558 therapeutics. *Br J Clin Pharmacol* **2014,** *77* (1), 63-71.
559 48. Mostafalu, P.; Kiaee, G.; Giatsidis, G.; Khalilpour, A.; Nabavinia, M.; Dokmeci, M. R.;
560 Sonkusale, S.; Orgill, D. P.; Tamayol, A.; Khademhosseini, A., A Textile Dressing for Temporal
561 and Dosage Controlled Drug Delivery. *Advanced Functional Materials* **2017,** *27* (41), 1702399.
562 49. Li, Y.; He, H.; Lu, W.; Jia, X., A poly(amidoamine) dendrimer-based drug carrier for
563 delivering DOX to gliomas cells. *RSC Advances* **2017,** *7* (25), 15475-15481.
564 50. Huang, C. L.; Kumar, S.; Tan, J. J. Z.; Boey, F. Y. C.; Venkatraman, S. S.; Steele, T. W.
565 J.; Loo, J. S. C., Modulating drug release from poly(lactic-co-glycolic acid) thin films through
566 terminal end-groups and molecular weight. *Polym. Degrad. Stabil.* **2013,** *98* (2), 619-626.
567 51. Steele, T. W. J.; Huang, C. L.; Kumar, S.; Iskandar, A.; Baoxin, A.; Boey, F. Y. C.; Loo,
568 J. S. C.; Venkatraman, S. S., Tuning drug release in polyester thin films: terminal end-groups

569 determine specific rates of additive-free controlled drug release. *Npg Asia Materials* **2013,** *5,*
570 e46.
571 52. Blencowe, A.; Fagour, W.; Blencowe, C.; Cosstick, K.; Hayes, W., Synthesis of
572 hyperbranched poly(aryl amine)s via a carbene insertion approach. *Org Biomol Chem* **2008,** *6*
573 (13), 2327-2333.
574 53. Moss, R. A.; Tian, J.; Chu, G.; Sauers, R. R.; Krogh-Jespersen, K., New mechanisms
575 centered on reactive intermediates: Examples from diazirine and carbene chemistry. *Pure and*
576 *Applied Chemistry* **2007,** *79* (6), 993-1001.
577 54. Moss, R. A., Diazirines: Carbene Precursors Par Excellence. *ACCOUNTS OF*
578 *CHEMICAL RESEARCH* **2006** *39* (4), 267-272.
579 55. Elson, C. M.; Liu, M. T. H., Electrochemical behaviour of diazirines. Journal of the
580 Chemical Society, Chemical Communications 1982, (7), 415-416.
581 56. Gale, D. M.; Middleton, W. J.; Krespan, C. G., Perfluorodiazo Compounds. *Journal of*
582 *the American Chemical Society* **1966,** *88* (15), 3617-3623.
583 57. Grayston, M. W.; Lemal, D. M., Perfluorohexamethylbicyclopropenyl. *Journal of the*
584 *American Chemical Society* **1976,** *98* (5), 1278-1280.
585 58. Michael T.H. Liu, K. R., Mechanism for the formation of azine in the decomposition of
586 diazo-alkanes and diazirines. *Tetrahedron Letters* **1977,** *36*, 3139 - 3142.
587 59. Pacheco, M. J.; Santos, V.; Ciríaco, L.; Lopes, A., Electrochemical degradation of
588 aromatic amines on BDD electrodes. *Journal of Hazardous Materials* **2011,** *186* (2), 1033-1041.
589 60. Adenier, A.; Chehimi, M. M.; Gallardo, I.; Pinson, J.; Vilà, N., Electrochemical
590 Oxidation of Aliphatic Amines and Their Attachment to Carbon and Metal Surfaces. *Langmuir*
591 **2004,** *20* (19), 8243-8253.

TABLE OF CONTENTS (TOC) GRAPHIC

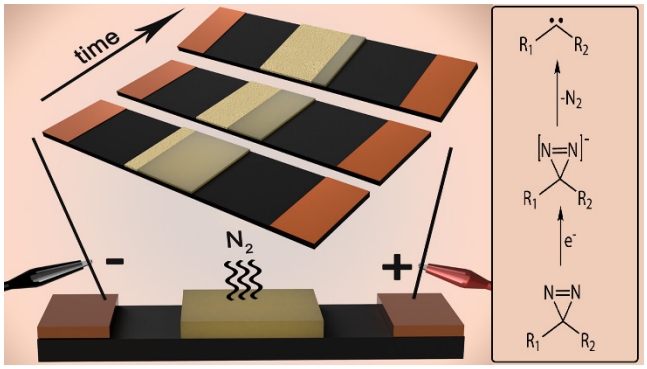

TABLE OF CONTENTS (TOC) SUMMARY

The electroceutical patch incorporates a bounded electric field that electrocures Voltaglue independent of position or surface area. For the first time, virtual bipolar electrodes are formed in-situ through the interface of Voltaglue and kiloohm per square hydrophobic resistive substrate. Milliamp currents activate an electrocuring zone of activation that is visually followable from the cathode to the anode on a minute timescale. Zone migration speed is variable by a few electrical and chemical parameters, offering a new tool for fixation of wound dressings and electroceutical interfaces.

Supporting Information

Voltaglue electroceutical adhesive patches for localized voltage stimulation

Manisha Singh[1,2], Richard D. Webster[3], Terry W. J. Steele[1,2]*

[1]NTU-Northwestern Institute for Nanomedicine (NNIN), Interdisciplinary Graduate School (IGS), Nanyang Technological University (NTU), 50 Nanyang Drive, Singapore 637553

[2]School of Materials Science and Engineering (MSE), Division of Materials Technology, Nanyang Technological University (NTU), Singapore 639798

[3]Division of Chemistry and Biological Chemistry, School of Physical and Mathematical Sciences, Nanyang Technological University, Singapore 637371

*Corresponding to Terry W. J. Steele (e-mail: wjsteele@ntu.edu.sg)

S1. Design and geometry of electroceutical patch

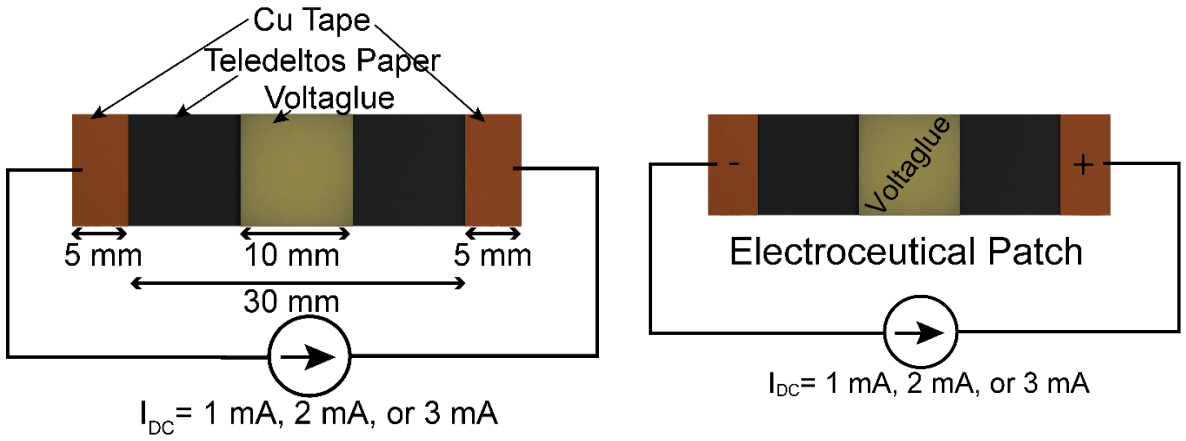

Figure S1: LEFT) Layout and dimensions of Teledeltos paper and Voltaglue placement within the bounded electric field. RIGHT) Composite semiconducting film, electrodes, and Voltaglue which serves as the electroceutical patch.

S2. Carbon sputter coating increases hydrophobicity

To test the speculation that aqueous formulation of Voltaglue might be delaminating the conductive coating, strips of the conductive paper are mounted on a stub and coated with a carbon layer using a sputter coater for 120 seconds. Hydrophobicity of the coated surfaces is tested using the OCA pro instrument (contact angle data physics, Germany). A 6 µL drop of pure distilled water is placed on the carbon paper surface both uncoated and carbon coated using a syringe with a 0.51 mm diameter needle. The measurements of each contact angle are performed within 5s after each drop to ensure that the droplet did not soak into the paper. The surface contact angles are the mean of the three determinations. The results displayed in the **Figure S2A** display that carbon coated conductive paper (120 s) shows a significant increase in contact angle when compared to uncoated conductive paper (increased from 78° to 100°).

The sheet resistance of the coated surfaces is measured using the four-point probe test. An average of 9 measurements is taken. The thickness of the paper is 0.18±0.02 mm. Both uncoated and coated conductive paper strips are tested and the results displayed in the **Figure S2B** display that sheet resistance has decreased from 4400 Ω sq^{-1} (uncoated) to 3940 Ω sq^{-1} (coated 120 s). However, the results are not significantly different.

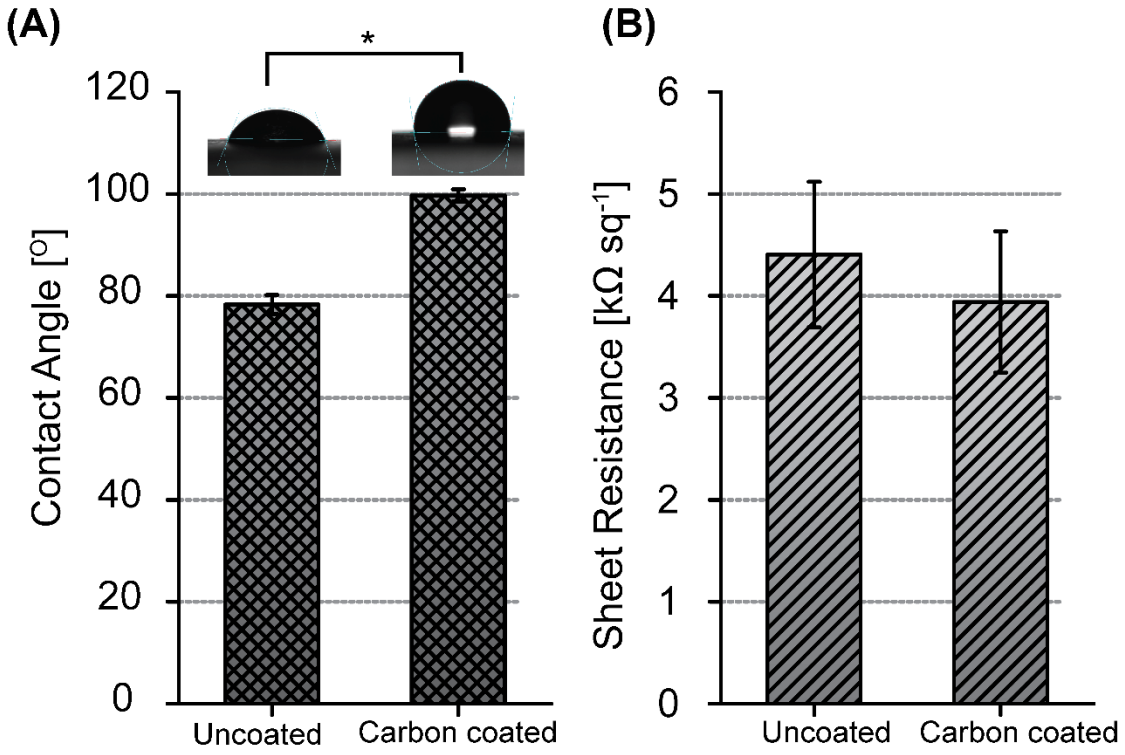

Figure S2: A) Surface contact angle measurements of the Teledeltos paper, B) Sheet resistance measurement of Teledeltos paper using a four-point probe test.

S3. Diffusion coefficients of ions

Table S1: Summary of ionic species within Voltaglue.

Species	**Amount (mmol)**	**Diffusion coefficient (m^2 s^{-1})[1-2]**	**Molar limiting conductivity of ion (S cm^2 mol^{-1})[1-2]**
Cl-	1.4	2.030	76.2
Na+	1.6	1.330	50
K+	0.045	1.960	73.6
PO_4^{3-}	0.12	0.612	206.8

[1] Table of Diffusion Coefficients. http://www.aqion.de/site/194.

[2] P. Vansek, "Ionic conductivity and diffusion at infinite dilution", CRC Handbook of Chemistry and Physics, 92th edition, ed. W. Haynes, (Boca Raton, Florida, CRC Press, 2011-2012) 5-76.